ASTM INTERNATIONAL
Standards Worldwide

Geotechnical
Testing Journal

A. Antriasian[1] and G. Beardsmore[2]

DOI: 10.1520/GTJ20130168

Longitudinal Heat Flow Calorimetry: A Method for Measuring the Heat Capacity of Rock Specimens Using a Divided Bar

VOL. 37 / NO. 5 / SEPTEMBER 2014

Geotechnical Testing Journal

doi:10.1520/GTJ20130168 / Vol. 37 / No. 5 / September 2014 / available online at www.astm.org

A. Antriasian[1] and G. Beardsmore[2]

Longitudinal Heat Flow Calorimetry: A Method for Measuring the Heat Capacity of Rock Specimens Using a Divided Bar

Reference

Antriasian, A. and Beardsmore, G., "Longitudinal Heat Flow Calorimetry: A Method for Measuring the Heat Capacity of Rock Specimens Using a Divided Bar," *Geotechnical Testing Journal*, Vol. 37, No. 5, 2014, pp. 859–868, doi:10.1520/GTJ20130168. ISSN 0149-6115

ABSTRACT

We present a method for measuring the heat capacity of a rock specimen using a divided bar apparatus in a "transient" mode. The specific heat capacity can be derived if the mass of the specimen is known. Thermal conductivity can be measured during a steady-state phase of the measurement process, and longitudinal thermal diffusivity can also be derived if the specimen volume (and hence density) is measured. A divided bar delivers a longitudinal flow of heat through a rock specimen and is conventionally used only in a steady-state mode for thermal conductivity measurements. Our method employs a time-series record of temperature changes at four points along the divided bar assembly to compare the net thermal energy absorbed by a specimen to its change in temperature during thermal re-equilibration from one steady-state temperature to another. The technique is calibrated using a set of analytical standards of known heat capacity. Our method yields mean values of specific heat capacity within ±1 % of published values for cultured quartz. Repeated measurements on the same specimens also give consistent results within approximately ±1 %. A combined thermal conductivity and heat capacity measurement takes less than one hour per specimen. Our method can be replicated with any divided bar apparatus employing a precise electronic temperature control system capable of switching between two steady-state mean temperatures, along with a digital data-logging system capable of recording and displaying data at a rate of one record per second.

Keywords

specific heat capacity, thermal petrophysics, calorimetry, thermal conductivity, divided bar

Manuscript received October 9, 2013; accepted for publication April 28, 2014; published online June 10, 2014.

[1] Hot Dry Rocks Pty Ltd, PO Box 251, South Yarra, VIC 3141, Australia (Corresponding author), e-mail: anson.antriasian@hotdryrocks.com

[2] Hot Dry Rocks Pty Ltd, PO Box 251, South Yarra, VIC 3141, Australia, e-mail: graeme.beardsmore@hotdryrocks.com

Introduction

THE THERMAL PROPERTIES OF ROCKS

The thermal properties of rocks are fundamental physical attributes that determine how the rocks behave in response to thermal loads. There are three basic, interrelated thermal properties: specific heat capacity, thermal conductivity, and thermal diffusivity.

The specific heat capacity (c_p) defines the amount of thermal energy required in order to raise or lower the temperature of one unit mass of material by one unit of temperature. It is a scalar quantity, insensitive to the direction of measurement. Within the context of Earth, c_p defines the ability of a geologic formation to store thermal energy. In planetary science, c_p is required for the calculation of thermal inertia [thermal inertia $= I = (\rho\lambda c_p)^{1/2}$, where ρ is density and λ is thermal conductivity], which controls the sensitivity of soil to changes in weather and insolation. Several methods have been developed for the measurement of c_p. Drop calorimetry requires heating a specimen to a known temperature and then transferring it into an immersion chamber with a fluid of known temperature and c_p, such that the temperature-versus-time curves of the fluid can be used to determine the net heat contributed by the specimen, such as described by Richet et al. (1982). Laser flash calorimetry (Parker et al. 1961; Takahashi et al. 1979) utilizes a laser beam as the heat source to add thermal energy to a specimen disk. The resulting increase in temperature is usually measured by a thermocouple contacting the specimen and is then used to calculate c_p, given that the mass or density is known. The laser flash apparatus is typically calibrated against a reference material of known c_p, and the specimen size is limited to several millimeters. Differential scanning calorimetry (Watson et al. 1964) calls for the simultaneous heating of both a specimen and a reference material while the differential energy required to keep them at the same temperatures during the linear scan is measured; the resulting heat flow curve can then be used to measure c_p and exothermic and endothermic reactions occurring with changes in temperature. Optical scanning uses a combined measurement of the thermal conductivity λ and the thermal diffusivity κ to calculate c_p (Popov et al. 1999).

Thermal conductivity (λ) controls the rate of heat transfer through a rock exposed to a thermal gradient. It is a tensor quantity that can have different values in different directions. Thermal conductivity measurements on drill core specimens have been used in conjunction with thermal gradient data for the measurement of crustal heat flow at least since the 1930s (Benfield 1939). With known heat flow, estimates of thermal conductivity allow temperature predictions at depths beyond what is accessible with wire-line logging. The thermal conductivity of wall rocks is also a critical parameter for designing ventilation systems for removing heat from mines and tunnels. Devices that have been developed to measure the thermal conductivity of rock specimens include the divided bar, the line source probe, optical scanning devices, hot-plate source apparatuses, and transient hot strip apparatuses.

Thermal diffusivity (κ) controls the rate at which an isothermal surface expands or contracts within a material in response to a point heat source or sink. Like thermal conductivity, thermal diffusivity is a tensor quantity. Typically, transient methods are used to directly measure thermal diffusivity by applying harmonic temperature cycles to one side of a specimen and measuring the phase change and amplitude decay of the cycle at a given distance and direction within the specimen. If the density (ρ), thermal conductivity (λ), and specific heat (c_p) are measured, thermal diffusivity can also be calculated according to the relationship (Carslaw and Jaeger 1959)

$$\kappa = \frac{\lambda}{\rho \cdot c_p} \tag{1}$$

In this paper we present a new method for measuring heat capacity using a divided bar apparatus. Coupled with a simple analytical scale to measure mass and volume, our method minimizes the specimen preparation and laboratory equipment required to determine all four parameters in Eq 1.

BACKGROUND ON THE DIVIDED BAR APPARATUS

Lodge (1878) first described the concept of a divided bar as a possible tool for measuring the thermal conductivity of rocks. Powell and Griffiths (1937) and Benfield (1939) developed early versions of the instrument by aligning two solid brass rods along their axes, separated by a disc-shaped specimen of the rock to be measured. The upper rod was heated and the lower rod cooled at their extreme ends, producing a flow of heat through the entire assembly.

Beck (1957) and Beardsmore and Cull (2001), among others, described improved versions of the divided bar with reduced lateral heat loss from the assembly. In those versions, a rock specimen is placed between two assemblies of brass–polycarbonate–brass plates (**Fig. 1**). The polycarbonate sheets provide a reference thermal conductivity, and the high-conductivity brass plates provide effective isothermal volumes of material for the physical placement of temperature sensors (typically thermocouples) at four points along the assembly. Each end of the assembly is maintained at a constant but different temperature so that a steady thermal gradient is applied across the whole assembly. The divided bar apparatus used in this trial is shown in **Fig. 2(*a*)**.

During a thermal conductivity measurement, the assembly approaches an equilibrium condition in which the temperatures T_1, T_2, T_3, and T_4 are constant and measureable [**Fig. 3(*a*)**]. At equilibrium, the ratio of the temperature differentials in Eq 2 is also constant [**Fig. 3(*b*)**] and directly related to the thermal conductivity of the specimen. One can derive the exact relationship

FIG. 1 Key components of the divided bar apparatus as described by Beardsmore and Cull (2001)—brass plates, polycarbonate disks, heat source, heat sink, and rock specimen. T_1, T_2, T_3, and T_4 are temperature measurement points using thermocouples with their weld joints embedded in the center of the brass plates. ΔT_1, ΔT_2, and ΔT_3 are the temperature differentials across the top polycarbonate disk, the rock specimen, and the bottom polycarbonate disk, respectively. Q_1, Q_2, and Q_3 represent the direction and magnitude of heat flow across the top polycarbonate disk, the rock specimen, and the bottom polycarbonate disk, respectively.

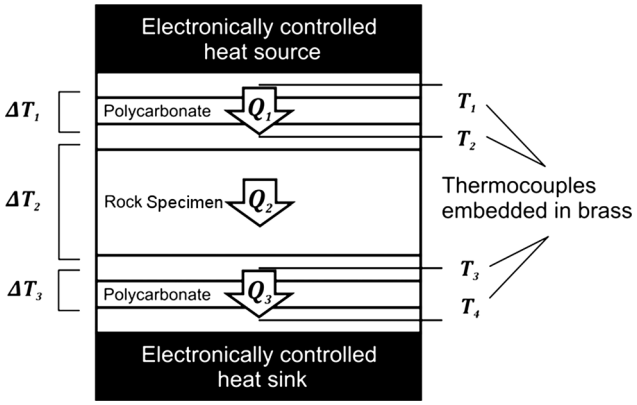

for any given divided bar by calibrating the apparatus using a range of specimens of different thickness and diameter and known conductivity.

$$\frac{\Delta T_2}{\Delta T_1 + \Delta T_3} \tag{2}$$

The divided bar has the ability to measure thermal conductivity along a single axis, so specimens can be prepared for measurement of thermal conductivity in the same direction as the natural flow of heat through the rock in situ. It is also well suited for measuring the "bulk" thermal conductivity of heterogeneous rock specimens, effectively averaging the effects of varying mineralogy, grain size, or porosity, or combinations thereof, within the specimen. These qualities contribute to the divided bar's utility in the 20th and 21st centuries for thermal conductivity measurements on rock specimens, despite the development of other devices based on transient heat pulses that can give more rapid measurements.

The divided bar is typically considered a "steady-state" device, providing a measurement of thermal conductivity only after thermal equilibrium has been attained. The authors are not aware of any previous attempt to use a divided bar to determine thermal properties other than thermal conductivity or to use a divided bar in a transient, or non-equilibrium, mode.

DIVIDED BAR APPARATUS USED IN THIS TRIAL

For this trial, the authors used a portable electronic divided bar (PEDB), as described by Antriasian (2010) [**Fig. 2(a)**]. The PEDB is in accord with the apparatus described in ASTM E1225-09. Like other divided bar designs, the PEDB holds a

FIG. 2 (a) A portable electronic divided bar (PEDB) as used in this trial. (b) View of PEDB with polyurethane foam thermal insulation in place.

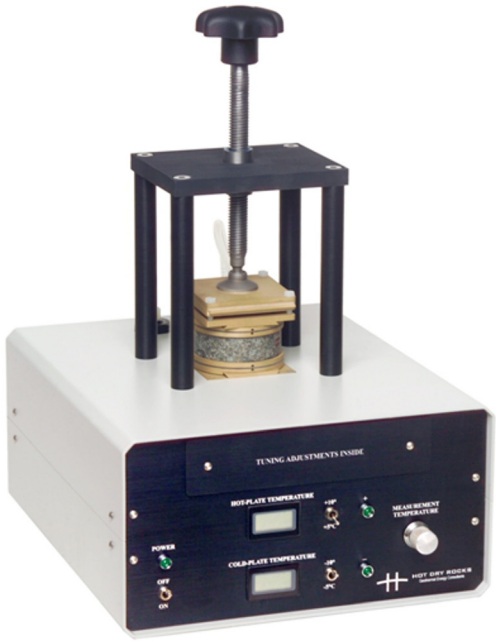

(a)

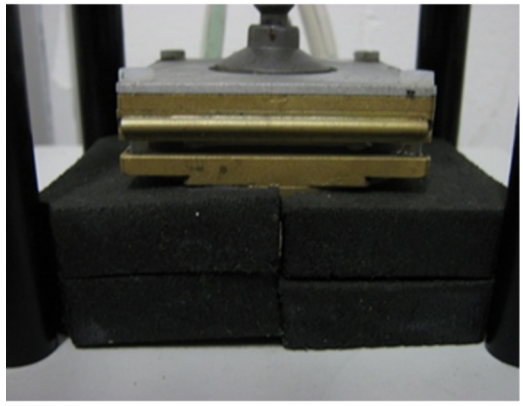

(b)

rock specimen between two brass–polycarbonate–brass assemblies. The rock specimen is typically a circular prism cut from a length of drill core, but the PEDB is also able to measure specimens of arbitrary shape and thickness, so long as they are prisms prepared with two approximately parallel flat surfaces contacting the brass plates. Depending on the specimen, a thermal conductivity measurement takes between 5 and 15 min.

The thermal gradient across the PEDB assembly is electronically maintained and controlled using Peltier thermoelectric heaters/coolers. Critical for the application we describe here, simple controls on the PEDB allow the operator to increase or decrease the mean temperature of the heat source and sink

FIG. 3 (a) Typical temperature trajectories at points T_1 (red), T_2 (orange), T_3 (green), and T_4 (blue) of a divided bar as it approaches thermal equilibrium following initiation of a thermal conductivity measurement at 100 s. (b) Evolution of the ratio $\Delta T_2/(\Delta T_1+\Delta T_3)$ during the measurement as illustrated in (a). In this case, the ratio equilibrated to a constant value of about 1.49 after about 300 s.

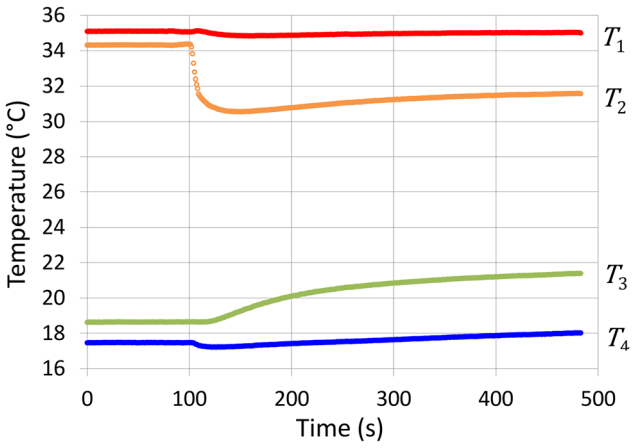

(a)

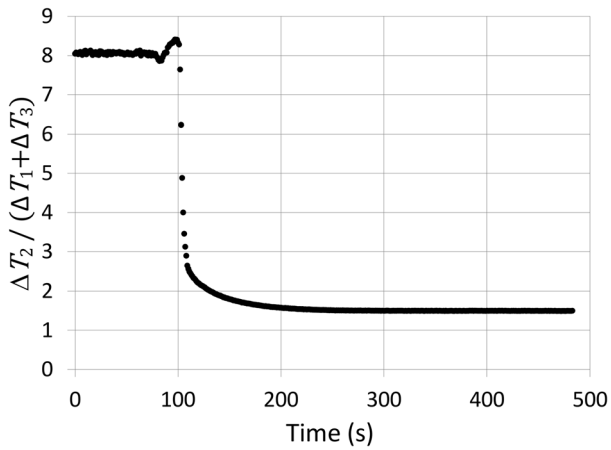

(b)

within a single measurement run while maintaining the same temperature differential across the assembly. A digital logging system records temperatures at each of the four measurement points (**Fig. 1**) to a resolution of 0.001°C at a rate of one set of readings per second.

In order for another divided bar device to be used to replicate the method for heat capacity measurements we describe in this paper, it would be critical that the device be able to deliver the following sequence of conditions (although the absolute values of temperature and temperature differential could vary). The assembly must first be brought to a steady-state condition with a thermal differential of about 20 K, and with the specimen held at a mean temperature of about 25°C (35°C at T_1, 15°C at T_4). The temperatures of the heat source and sink must then be simultaneously raised to increase the mean temperature of the specimen to about 35°C while maintaining the thermal differential at 20 K (45°C at T_1, 25°C at T_4). The temperature trajectories at T_1, T_2, T_3, and T_4 must be recorded during the entire process to a resolution of approximately 0.001°C at a rate of approximately one set of readings per second.

FIG. 4 Following equilibration of the measurement shown in **Fig. 3**, temperatures at points T_1 (red) and T_4 (blue) are simultaneously reset to higher values at 100 s on this graph. The temperatures at points T_2 (orange) and T_3 (green) record the subsequent re-equilibration of the mean specimen temperature $[(T_2+T_3)/2]$ from about 26.9°C to 33.7°C.

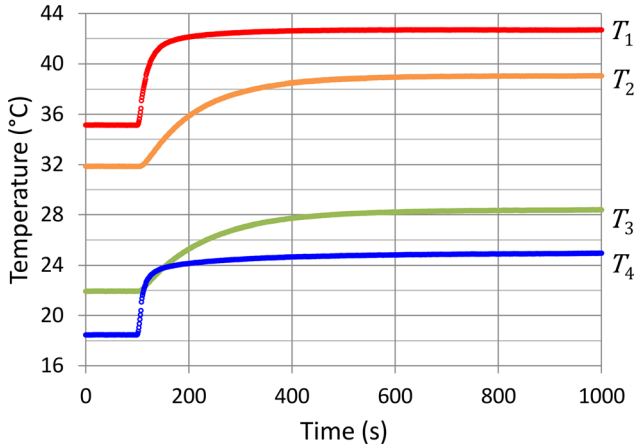

Theoretical Basis of Method

We describe here a method for measuring the heat capacity of a rock specimen using a divided bar apparatus, as an additional measurement to complement the conventional thermal conductivity measurement. Our tactic is to monitor the thermal energy absorbed by a specimen as it increases in temperature by a known amount. We start with Fourier's law, which states that linear heat flow within a given body can be described by (Carslaw and Jaeger 1959)

$$Q = A\lambda\frac{\Delta T}{l} \tag{3}$$

where:

Q = rate of heat flow through the body, W or J/s,

A = cross-sectional area of the body normal to heat flow, m^2,

λ = thermal conductivity of the body, W/(mK),

ΔT = temperature differential across the body, K, and

l = thickness of the body parallel to heat flow, m.

When a rock specimen is placed in a divided bar and brought to thermal equilibrium (i.e., T_1, T_2, T_3, and T_4 remain constant over time as shown in **Fig. 4**, from 700 to 1000 s), the First Law of Thermodynamics ("conservation of energy") dictates that the rate of heat flow at equilibrium is constant across the upper polycarbonate, the rock specimen, and the

lower polycarbonate (assuming axial heat flow with no side loss).

$$Q_1 = Q_2 = Q_3 \tag{4}$$

Substituting Eq 3 into Eq 4 gives

$$A_1 \frac{\lambda_1}{l_1} \Delta T_1 = A_2 \frac{\lambda_2}{l_2} \Delta T_2 = A_3 \frac{\lambda_3}{l_3} \Delta T_3 \tag{5}$$

where:

A_1 and A_3 = cross-sectional area of divided bar assembly, m^2,

A_2 = cross-sectional area of rock specimen, m^2,

λ_1 and λ_3 = thermal conductivity of top and bottom polycarbonate disks, W/(mK),

λ_2 = thermal conductivity of rock specimen, W/(mK),

l_1 and l_3 = thickness of top and bottom polycarbonate disks, m, and

l_2 = thickness of rock specimen, m.

In practice, the ratios $(A_1\lambda_1)/l_1$ and $(A_3\lambda_3)/l_3$ are constants and virtually equal for a given divided bar apparatus. They can be derived via calibration using specimens with known values of A_2, λ_2, and l_2.

At thermal equilibrium, the rock specimen is at a mean temperature of approximately $(T_2 + T_3)/2$, where T_2 and T_3 are the temperatures at the points indicated in **Fig. 1**. If T_1 and T_4 are simultaneously increased, the entire divided bar assembly, including the rock specimen, increases in temperature over time to a new thermal equilibrium condition (**Fig. 4**). The total quantity of heat absorbed by the specimen during the large time re-equilibration process is the product of the heat capacity $(c_p m_s)$ and the increase in mean temperature of the specimen.

$$\Delta H = c_p m_s \Delta \left(\frac{T_2 + T_3}{2} \right) \tag{6}$$

where:

ΔH = change in stored thermal energy in the specimen, J,

m_s = mass of the specimen, kg,

c_p = specific heat capacity of the specimen, J/(kgK), and

$\Delta[(T_2 + T_3)/2]$ = change in mean temperature of the specimen, K.

The increase in thermal energy within the specimen (ΔH) is brought about by an imbalance between the heat flowing into the specimen (Q_1) and the heat flowing out of the specimen (Q_3) during the re-equilibration period. For simple systems of steady-state heat flow, the net heat that has been transferred (ΔH) can be calculated by taking the product of the rate of heat transfer (Q) and the time duration of the heat transfer ($t_f - t_0$), algebraically described as $\Delta H = Q(t_f - t_0)$. This is similar to how the net energy exerted in an electrical circuit (watt seconds) can be calculated as the product of the output power (watts) and the time duration of applied power (seconds). But because Q for our divided bar is nonconstant over the time interval of our specific heat measurement, such a simple formula is not suitable for calculating ΔH from Q. Instead, the fundamental theorem of calculus is applied, such that the sum of infinitesimal changes in Q with time provides the net change in ΔH over the time interval $(t_f - t_0)$. So ΔH can be described for large times in terms of time integrals of Q_1 and Q_3.

$$\Delta H = \int_{t_0}^{t_f} Q_1 dt - \int_{t_0}^{t_f} Q_3 dt \tag{7}$$

where:

t_0 = instant at which T_1 and T_4 are increased, s,

t_f = instant at which re-equilibration is reached, s, and

Q_1 and Q_3 = as defined in Eqs 3 and 4, J/s.

Re-equilibration is defined as the point at which the thermal states of the divided bar and the specimen become sufficiently close to the large time state and there is no longer an imbalance between the heat flowing into the specimen (Q_1) and the heat flowing out of the specimen (Q_3). This is shown in **Fig. 5** as the value of $(\Delta T_1 - \Delta T_3)$ becomes sufficiently close to 0 K, occurring at about 900 s.

If we replace Q with the variables from Eq 3, we get

$$\Delta H = \frac{A\lambda}{l} \left[\int_{t_0}^{t_f} \Delta T_1 dt - \int_{t_0}^{t_f} \Delta T_3 dt \right] \tag{8}$$

or

$$\Delta H = \frac{A\lambda}{l} \left[\int_{t_0}^{t_f} (\Delta T_1 - \Delta T_3) dt \right] \tag{9}$$

FIG. 5 Evolution of $[\Delta T_1 - \Delta T_3]$ (black) and the change in mean specimen temperature $\Delta(T_2 + T_3)/2$ (gray) for the record shown in **Fig. 4**. The area between the back curve and the time axis is proportional to the total heat energy absorbed by the specimen as it increases in temperature by about 6.8 K. Re-equilibration is defined as the approach of $[\Delta T_1 - \Delta T_3]$ to a value sufficiently close to 0 K, which was complete by about the 900-s mark, or 800 s after the temperatures of the heat source and sink were increased.

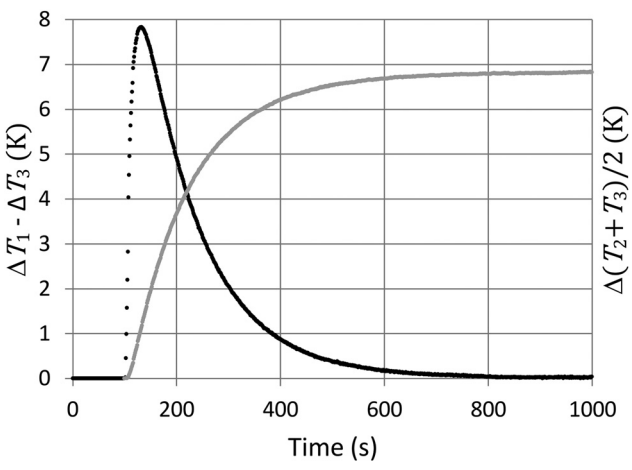

where:

$(A\lambda)/l$ = a constant derived through calibration of the divided bar, and

ΔT_1 and ΔT_3 = the temperature differentials shown in **Fig. 1**.

The above relationships all assume that the temperature changes within the device and specimen during re-equilibration cause no significant change in the value of A, λ, or l for the divided bar components or rock specimen.

Combining Eq 6 with Eq 9 yields a function for the heat capacity of the specimen ($c_p m_s$) in terms of recorded temperatures and calibration constants.

$$c_p m_s \Delta\left(\frac{T_2 + T_3}{2}\right) = \frac{A\lambda}{l}\left[\int_{t_0}^{t_f} (\Delta T_1 - \Delta T_3)dt\right]$$

or

$$c_p m_s = \frac{\frac{A\lambda}{l}\int_{t_0}^{t_f} [\Delta T_1 - \Delta T_3]dt}{\Delta\left(\frac{T_2 + T_3}{2}\right)} \quad (10)$$

where the following are easily measured or derived:

$(A\lambda)/l$ = calibration constant for the divided bar, and

$\Delta[(T_2 + T_3)/2]$ = observed change in the mean specimen temperature.

In practice, temperatures are recorded at regular discrete time intervals, so the integral in Eq 10 is better redefined as

$$\int_{t_0}^{t_f} [\Delta T_1 - \Delta T_3]dt = \Delta t \sum_{t_0}^{t_f} [\Delta T_1 - \Delta T_3] \quad (11)$$

where:

Δt = the discrete time interval between temperature readings, s, and

$[\Delta T_1 - \Delta T_3] = [(T_1 - T_2) - (T_3 - T_4)]$ as defined in **Fig. 1**, K.

Figure 5 shows how $[\Delta T_1 - \Delta T_3]$ varies through time during the measurement shown in **Fig. 4**. The area between the curve and the time axis on **Fig. 5** is the graphical equivalent of the integral in Eq 11. The value of the integral (in K · s) can be calculated arithmetically for any given measurement by summing all the records of $[\Delta T_1 - \Delta T_3]$ over the re-equilibration time interval and multiplying the sum by Δt. The value can then be inserted into Eq 10 along with the other measured variables and constants to calculate the heat capacity of the specimen. Division by the mass of the specimen yields the specific heat capacity.

The method described above requires that a measurement reach full re-equilibration before the heat capacity of the specimen can be calculated. However, a different treatment of the recorded temperature data allows the heat capacity to be derived before full equilibration is reached, allowing more rapid measurements.

Consider the relationship described by Eq 10, as modified by Eq 11.

$$c_p m_s = \frac{A\lambda}{l}\left\{\Delta t \sum_{t_0}^{t_n} [\Delta T_1 - \Delta T_3] / \Delta\left(\frac{T_2 + T_3}{2}\right)\right\} \quad (12a)$$

Or, equivalently,

$$c_p m_s = \frac{A\lambda}{l}\left\{\Delta t \sum_{t_0}^{t_n} [\Delta T_1 - \Delta T_3] \Big/ \left[\left(\frac{T_2 + T_3}{2}\right)_n - \left(\frac{T_2 + T_3}{2}\right)_0\right]\right\} \quad (12b)$$

All of the parameters outside of the braces in Eq 12 are constants, which implies that the term inside the braces must also be a constant or converge to a constant over time. The term inside the braces represents the "total amount of heat added to the specimen, divided by the change in temperature of the specimen." However, $[(T_2 + T_3)/2]_n$ does not accurately represent the mean temperature of the specimen at short times after increasing the temperatures of the heat source and sink, because the temperature gradient through the specimen is initially nonlinear. This nonlinearity is a result of rapid heating of the contact surfaces of the specimen while the core of the specimen lags in temperature response because of its finite thermal diffusivity.

This phenomenon also occurs within the brass and polycarbonate plates, so that the temperature gradients across the divided bar components are nonlinear for small times after the temperature increase. This can be noted in **Fig. 4**, which shows a rapid increase in the temperature of the heat source and sink (T_1 and T_4) and a much more gradual increase in the temperature of the plates contacting the specimen (T_2 and T_3) due to the finite thermal diffusivity of the brass and polycarbonate plates, and to the heat being absorbed by the specimen; specimens with large heat capacities have been observed to take longer to re-equilibrate. It follows that Eq 12 does not give a reliable result for $c_p m_s$ at small values of t_n. With increasing time, the temperature gradient through the specimen and divided bar components approaches linearity, $[(T_2 + T_3)/2]_n$ approaches an accurate representation of the mean specimen temperature, and Eq 12 converges on a reliable value of $c_p m_s$.

Figure 6 shows the evolution of $(T_2 + T_3)/2$ with increasing time for the example illustrated in **Figs. 4** and **5**. It illustrates the convergence described in the previous paragraph and suggests that, in this example at least, a measurement of $c_p m_s$ could be completed in about half the time required for full thermal re-equilibration of the divided bar.

Calibration

The discussion above theorizes that for an ideal divided bar apparatus it is possible to derive the heat capacity of an unknown

FIG. 6 Evolution of the term in braces in Eq 12 for the temperature records shown in **Figs. 4** and **5**. The term stabilized at a constant value of about 175.4 (gray) around 350 s after the temperatures of the heat source and sink were increased (100 s for this example), or about half the time of full thermal re-equilibration of the divided bar.

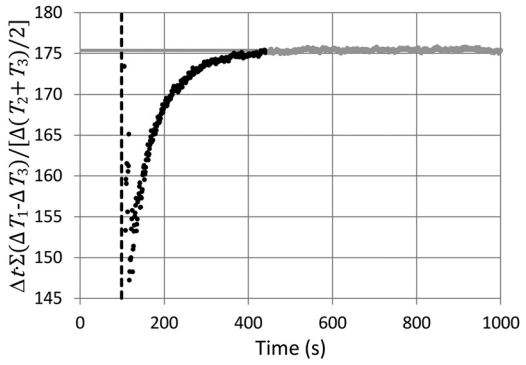

specimen from a time series record of a thermal re-equilibration process. According to Eq 12, however, we also need to know the values of certain physical properties of the divided bar apparatus itself. Specifically, Eq 12 requires the surface area (A), thermal conductivity (λ), and thickness (l) of the polycarbonate sheets as shown in **Fig. 1**. In practice, we do not need to know the absolute values of these parameters; only the ratio $(A\lambda)/l$ as appears in Eq 12 is required. This can be derived through a calibration procedure.

For an ideal divided bar apparatus, a single measurement of a reference standard of known heat capacity would be sufficient to calibrate the device. We would know the values of $c_p m_s$ and Δt for that single measurement and could easily derive $[(A\lambda)/l]$ by plotting the thermal re-equilibration data on a graph such as in **Fig. 6**.

In reality, though, no divided bar apparatus is "ideal." Significantly, our theoretical treatment up to Eq 12 implicitly assumes that the temperature differential ΔT_2 (**Fig. 1**) exactly represents the temperature drop across the specimen being measured. Most practical divided bar apparatuses have the temperature measurement points T_2 and T_3 embedded within disks of a highly conductive metal such as brass. The apparatus we used is no exception. Every measurement inherently incorporates a finite thickness and mass of brass in the interval between the T_2 and T_3 measurement points. The heat capacity of the brass component effectively adds another constant to the relationship in Eq 12.

$$c_p m_s = \frac{A\lambda}{l}\left\{\Delta t \sum_{t_0}^{t_n}[\Delta T_1 - \Delta T_3]/\Delta\left(\frac{T_2+T_3}{2}\right)\right\} - C_b \quad (13)$$

where:

C_b = heat capacity of the brass between points T_2 and T_3 in **Fig. 1**.

Equation 13 describes a linear relationship between $c_p m_s$ and the term in braces. The relationship has a slope of $(A\lambda)/l$ and a y-intercept of $-C_b$. The calibration procedure involves finding the equilibrium values of the term in braces for reference standards with at least two (but preferably more) different values of $c_p m_s$ to define a straight line. We used three circular windows of KU-1 high-purity fused silica as reference standards, all of the same diameter, but with different thicknesses. We derived the heat capacity of the standards from molar heat capacity values published by Richet et al. (1982) for high-purity fused silica (**Table 1**) and chose the thicknesses to cover the expected range of heat capacities of rock specimens we would typically measure.

TABLE 1 Molar heat capacity of high-purity fused silica published for different temperatures by Richet et al. (1982). We assumed a molar weight of 60.0855 g/mol for SiO_2 to derive a specific heat capacity relationship with temperature for KU-1 high-purity fused silica windows.

Temperature, K	Molar Heat Capacity, J/(mol · K)	Specific Heat Capacity, J/(kg · K)
273	41.465	690
298	44.061	733
300	44.243	736
400	52.392	872

Table 2 gives the precise dimensions and heat capacities of the reference standards we used and the respective equilibrium values we recorded for the term in braces in Eq 13. **Figure 6** shows a graph of the three calibration points, the straight line of best fit through those points, and the derived values of $(A\lambda)/l$ and C_b. Our calibration equation is thus

$$c_p m_s = 0.593 \times \left\{\Delta t \sum_{t_0}^{t_n}[\Delta T_1 - \Delta T_3]/\Delta\left(\frac{T_2+T_3}{2}\right)\right\} - 67.7 \quad (14)$$

The derived value of C_b, 67.7 J/K, is within a few percent of 65.8 J/K, the predicted heat capacity of a disk of brass [density = 8700 kg/m^3, c_p = 380 J/(kg K)] of 65-mm diameter and 6-mm thickness, which closely matches the dimensions of the brass disks in our divided bar apparatus. Suspected reasons for the slight disagreement between the derived and the predicted heat capacity of brass include variability in brass composition, environmental heat loss, idiosyncrasies within the thermocouple data logger, variability in brass plate geometry, and the influence of the 1-mm-diameter polymer-filled thermocouple embedding holes.

Examples

To test our methodology, we measured the heat capacity and derived the specific heat capacity of three "unknown" specimens of the same diameter as the calibration reference standards. The three specimens were a KU-1 fused silica window of a different thickness than the reference standards, a window of cultured

TABLE 2 Calibration data for KU-1 fused silica windows as plotted in **Fig. 7**. Assumes a specific heat capacity of 743 J/(kg · K) for KU-1 fused silica at 31°C, from **Table 1**.

Diameter, m	Thickness, m	Measured Mass, kg	Heat Capacity, J/K	Equilibrium $\Sigma(\Delta T_1 - \Delta T_3)/[\Delta(T_2 + T_3)/2]$
0.04796	0.0083	0.0332	24.65	155.75
0.04796	0.0163	0.0648	48.14	195.20
0.04796	0.0253	0.1005	74.63	240.00

quartz, and a disk of 316 stainless steel. We repeated the measurements of each specimen three times to investigate the repeatability of the results. We carried out the following sequence for each of the nine measurements.

1. Measure the mass m_s of the specimen using an analytical scale.
2. Insert the specimen into the divided bar and allow the apparatus to attain thermal equilibrium at a mean specimen temperature of about 25°C, following the normal procedure for a thermal conductivity measurement. This places the specimen into a thermal state similar to that represented by the time interval preceding the 100-s mark in **Fig. 4**.
3. Simultaneously increase the temperatures of the hot and cold plates (**Fig. 1**) to a state approximately 10 K higher. This was achieved on the PEDB with the turn of a dial.
4. Log the resulting disturbance and re-equilibration of temperatures T_1, T_2, T_3, and T_4 (**Fig. 4**) at 1-s intervals.
5. Monitor the progression of the parameter in braces in Eq 14 (**Fig. 6**) until it stabilizes to a constant value.
6. Insert the constant value obtained in step 5 into Eq 14 to calculate $c_p m_s$.
7. Divide by the mass of the specimen from step 1 to derive c_p.

Our results are shown in **Table 3**, along with the average and standard deviation of the three measurements for each specimen and the "expected" value of the specific heat capacity based on previously published data. Each individual measurement returned a value within about ± 2 % of the expected value, and the mean values were within about ±1 % of those expected.

TABLE 3 Results of three independent measurements of specific heat capacity for each of three "unknown" specimens, with arithmetic mean and one standard deviation (σ) for each specimen. "Expected values" for KU-1 fused silica and cultured quartz are from data published by Richet et al. (1982). The end-members of the range of expected values for 316 stainless steel are from Bogaard et al. (1993) and Sandvik (2013).

	c_p, J/(kg · K)					
Specimen	Trial 1	Trial 2	Trial 3	Mean	σ	Expected Value
KU-1 fused silica	747	740	736	741	6	746
Cultured quartz	751	743	741	745	5	754
316 stainless steel	464	462	460	462	2	450–490

The repeatability of our method, as represented by the standard deviations of the results, appears to be better than ±1 %.

Practical Considerations

In this paper we have demonstrated an ability to measure the heat capacity of rock specimens by operating a divided bar apparatus in a "transient" mode, rather than the usual steady-state mode for which it was originally designed. A critical component of the system is a digital logger that is able to simultaneously measure, record, partially process, and display the ratios of temperatures at four different points along the divided bar at regular time intervals (for example, one set of measurements per second.) We utilized a commercially available thermocouple data logger with eight channels and associated operating software. The software allowed real-time on-screen presentation of the relevant parameters, allowing us to monitor when a specimen had attained thermal equilibrium.

Through experience, we have found that full thermal re-equilibration (as shown in **Fig. 5**) typically takes 25 to 30 min from the instant at which the temperatures of the heat source and sink are increased. Stabilization to a measureable value as illustrated in **Fig. 6**, however, typically takes only 10 to 15 min. The measurement time for any given specimen depends on its heat capacity, with lower-heat-capacity specimens equilibrating faster.

Figure 5 represents an ideal situation in which the parameter $[\Delta T_1 - \Delta T_3]$ begins at zero and re-equilibrates back to zero after the heat source and sink temperatures are increased. In practice, $[\Delta T_1 - \Delta T_3]$ usually equilibrates to plus or minus a few tenths of a Kelvin, and there is often an offset between "before" and "after" equilibrium values of $[\Delta T_1 - \Delta T_3]$, regardless of how long a measurement continues. **Figure 8*(a)*** shows the trajectory of $[\Delta T_1 - \Delta T_3]$ recorded during a real measurement. In this example, $[\Delta T_1 - \Delta T_3]$ equilibrated to − 0.196 K before the temperatures were increased and 0.194 K after the increase.

The reasons for the non-zero equilibrium values and offsets are not immediately evident but possibly relate to different amounts of radial heat loss from the specimen and divided bar at different temperatures, asymmetry in the positions of the thermocouples embedded in the brass plates, or idiosyncrasies within the thermocouple data logger. The presence of thermal insulation around the apparatus to prevent radial heat transfer

during a measurement appears to influence the magnitude of the equilibrium values and offsets. Transient thermal effects such as variations in laboratory temperature reduce the quality of equilibration curves such as those shown in **Figs. 5** and **6** and consequently reduce measurement quality, and so it is recommended that one maximize the thermal insulation used and minimize variation in laboratory temperature during measurement. **Figure 2(*b*)** shows the thermal insulation configuration used for the experiments presented herein.

In practice, we use the value of $[\Delta T_1 - \Delta T_3]$ *after* re-equilibration as the baseline [solid horizontal line on **Fig. 8(*a*)**] for calculating the sum $\sum[\Delta T_1 - \Delta T_3]$ as referred to in Eq 14. Although a sample can be allowed to fully re-equilibrate its final value of $[\Delta T_1 - \Delta T_3]$, which can be used to calculate $\sum[\Delta T_1 - \Delta T_3]$, a method exists that enables specific heat measurement before full re-equilibration.

Figure 8(*b*) shows the evolution of the term in braces in Eq 14 versus time for the record shown in **Fig. 8(*a*)**. It is evident that the graph converges toward a line with a positive slope [gray in **Fig. 8(*b*)**], rather than a horizontal line as in **Fig. 6**. To investigate why this is the case, we can mathematically represent the term plotted in **Fig. 8(*b*)** as

$$\frac{\sum_{i=0}^{n} \Delta t[\Delta T_1 - \Delta T_3]_i}{\Delta\left(\frac{T_2 + T_3}{2}\right)_n} = \frac{\sum_{i=0}^{n} \Delta t[R_i + F]}{\Delta\left(\frac{T_2 + T_3}{2}\right)_n} \quad (15)$$

where:

$i = 0$ = instant at which heat source and sink temperatures increase,

R_i = difference between the observed $[\Delta T_1 - \Delta T_3]$ and F at any given time, and

F = difference between the initial value of $[\Delta T_1 - \Delta T_3]$ and the final re-equilibrated value of $[\Delta T_1 - \Delta T_3]$.

Graphically, F is the difference between the solid and dashed horizontal lines in **Fig. 8(*a*)**. The right-hand side of Eq 15 can be split into two parts describing a linear function with time t.

$$\frac{\sum_{i=0}^{n} \Delta t[R_i + F]}{\Delta\left(\frac{T_2 + T_3}{2}\right)_n} = \frac{\Delta t \sum_{i=0}^{n} R_i}{\Delta\left(\frac{T_2 + T_3}{2}\right)_n} + \frac{tF}{\Delta\left(\frac{T_2 + T_3}{2}\right)_n} \quad (16)$$

This means that a measurement need only proceed until a linear trend as described by Eq 16 can be identified and the "intercept" can be quantified on a plot such as that in **Fig. 8(*b*)**. The

FIG. 7 Calibration points and straight line of best fit derived from three different thicknesses of KU-1 fused silica windows of 47.96-mm diameter. The three points define a straight line to a very high precision ($R^2 = 1.000$), giving the two calibration coefficients for this device.

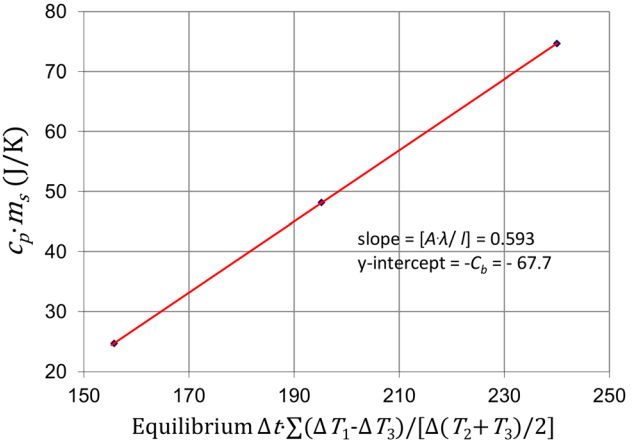

FIG. 8 (a) An example of $[\Delta T_1 - \Delta T_3]$ (black) equilibrating to different non-zero steady-state values before (dashed horizontal line) and after (solid horizontal line) a change in mean specimen temperature by 6.8 K (gray). (b) $\Delta t\sum[\Delta T_1 - \Delta T_3]/[\Delta(T_2 + T_3)/2]$ versus time approaches linearity as described by Eq 16. The data from 350 s to 600 s were used to define the gray line, the intercept of which with the instant of temperature increase (vertical dashed line) gives $\Delta t\sum[\Delta T_1 - \Delta T_3]/[\Delta(T_2 + T_3)/2] = 175.4 \pm 2$ for input into Eq 14.

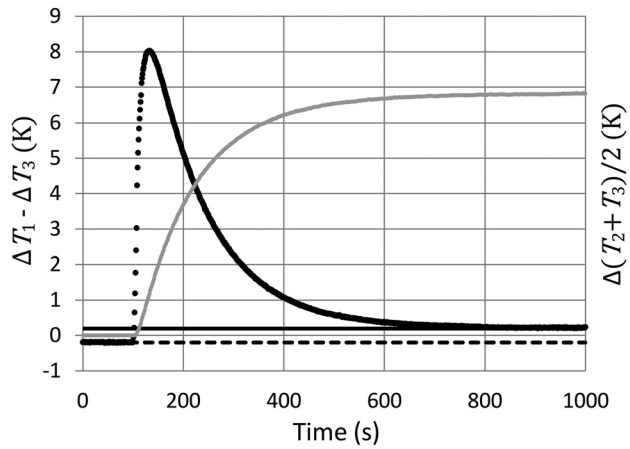

(a)

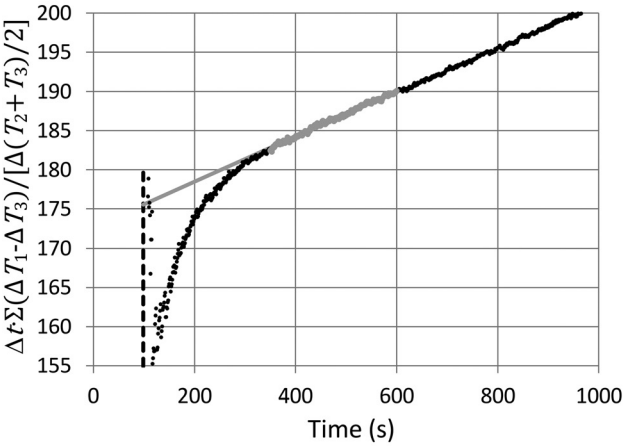

(b)

intercept term on the right-hand side of Eq 16 is the relevant value for input into Eq 14 or **Fig. 7**. The "slope" term, the rightmost term on the right-hand side of Eq 16, is directly proportional to the final equilibrated value of $[\Delta T_1 - \Delta T_3]$ [solid horizontal line in **Fig. 8(*a*)**] but is irrelevant to the calculation of heat capacity.

Conclusions

We have presented a method for measuring the heat capacity of a rock specimen using a divided bar apparatus in a "transient" mode. The methodology gives mean results to within ±1 % of published values of standard materials (specifically cultured quartz and fused silica glass), and results on the same specimen are repeatable to within ±1 %. Along with an analytical balance to measure mass and density, the method allows specific heat capacity and thermal diffusivity to also be derived with a minimum of equipment.

The methodology for a heat capacity measurement described above involves increasing the mean temperature of a rock specimen while maintaining a constant temperature differential of about 20 K across the divided bar. This procedure allows concurrent measurement of thermal conductivity at the steady-state condition preceding an increase in mean specimen temperature. The same methodology can be successfully applied by decreasing the mean specimen temperature. It would also be feasible to measure heat capacity by increasing or decreasing the mean temperature of the specimen from a starting condition of homogeneous temperature through the divided bar, but at the cost of losing a concurrent thermal conductivity measurement.

References

Antriasian, A., 2010, "The Portable Electronic Divided Bar (PEDB): A Tool for Measuring Thermal Conductivity of Rock Samples," *Proceedings of the World Geothermal Congress 2010, Indonesia*, International Geothermal Association, Lennershofstr. 140, D-44801 Bochum, GERMANY.

ASTM E1225-09: Thermal Conductivity of Solids by Means of the Guarded-Comparative-Longitudinal Heat Flow Technique, *Annual Book of ASTM Standards*, ASTM International, West Conshohocken, PA, 2009.

Beardsmore, G. R. and Cull, J. P., 2001, *Crustal Heat Flow: A Guide to Measurement and Modelling*, Cambridge University Press, Cambridge, UK, p. 108.

Beck, A., 1957, "A Steady State Method for the Rapid Measurement of the Thermal Conductivity of Rocks," *J. Sci. Instrum.*, Vol. 34, No. 5, pp. 186–189.

Benfield, A. E., 1939, "Terrestrial Heat Flow in Great Britain," *Proc. R. Soc. London Ser. A, Math. Phys. Sci.*, Vol. 173, No. 955, pp. 428–450.

Bogaard, R. H., Desai, P. D., Li, H. H., and Ho, C. Y., 1993, "Thermophysical Properties of Stainless Steels," *Thermochim. Acta*, Vol. 218, pp. 373–393.

Carslaw, H. S. and Jaeger, J. C., 1959, *Conduction of Heat in Solids*, 2nd ed., Oxford University Press, Oxford, UK, pp. 7–9.

Lodge, O. J., 1878, "On a Method of Measuring the Absolute Thermal Conductivity of Crystals and Other Rare Substances—Part I," *Philos. Mag. Ser. 5*, Vol. 5, No. 29, pp. 110–117.

Parker, W. J., Jenkins, R. J., Butler, C. P., and Abbott, G. L., 1961, "Method of Determining Thermal Diffusivity, Heat Capacity and Thermal Conductivity," *J. Appl. Phys.*, Vol. 32, No. 9, p. 1679.

Popov, Y. A., Pribnow, D. F. C., Sass, J. H., Williams, C. F., and Burkhardt, H., 1999, "Characterization of Rock Thermal Conductivity by High Resolution Optical Scanning," *Geothermics*, Vol. 28, No. 2, pp. 253–276.

Powell, R. W. and Griffiths, E., 1937, "The Variation with Temperature of the Thermal Conductivity and the X-ray Structure of Some Micas. I. The Thermal Conductivity up to 600°C," *Proc. R. Soc. London Ser. A, Math. Phys. Sci.*, Vol. 163, No. 913, pp. 189–198.

Richet, P., Bottinga, Y., Denielou, L., Petitet, J. P., and Tequi, C., 1982, "Thermodynamic Properties of Quartz, Cristobalite and Amorphous SiO_2: Drop Calorimetry Measurements between 1000 and 1800 K and a Review from 0 to 2000 K," *Geochim. Cosmochim. Acta*, Vol. 46, No. 12, pp. 2639–2658.

Sandvik, 2013, "Sanmac 316/316L," Physical Property Data Sheet for 316 stainless steel, http://www.smt.sandvik.com/en/materials-center/material-datasheets/bar-and-hollow-bar/bar/sanmac-316316l/ (Last accessed 23 Sept 2013).

Takahashi, Y., Yokokawa, H., Kadokura, H., Sekine, Y., and Mukaibo, T., 1979, "Laser Flash Calorimetry I. Calibration and Test of Alumina Heat Capacity," *J. Chem. Thermodynamics*, Vol. 11, No. 4, pp. 379–394.

Watson, E. S., O'Neill, M. J., Justin, J., and Brenner, N., 1964, "A Differential Scanning Calorimeter for Quantitative Differential Thermal Analysis," *Anal. Chem.*, Vol. 36, No. 7, pp. 1233–1238.